Supporting Information

Dai et al. 10.1073/pnas.1220711110

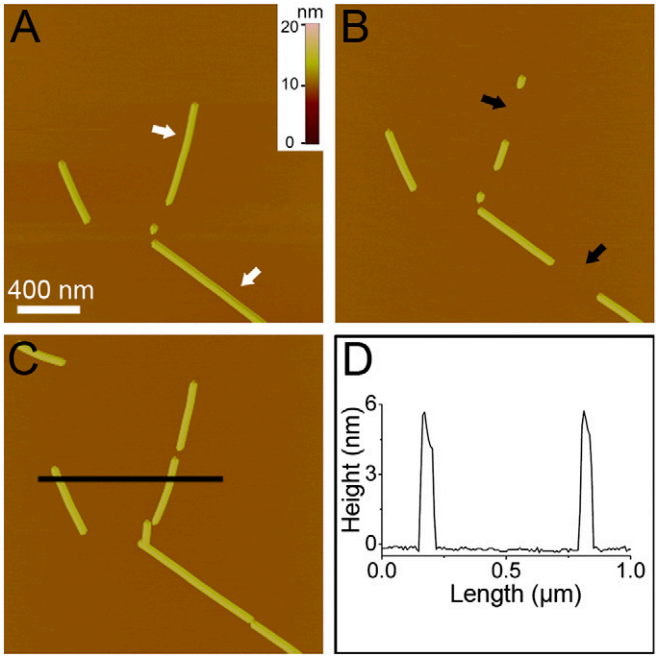

Fig. S1. Tapping mode atomic force microscopy (AFM) height images and section profile indicating the extension of double-layered NH_2-VGGAVVAGV-$CONH_2$ (GAV-9) nanofilaments after removing two parts from the preformed double-layered nanofilaments. (*A*) Original double-layered GAV-9 nanofilaments. (*B*) Gaps appeared on the original nanofilaments after AFM mechanical manipulation at the positions indicated with black arrows. (*C*) GAV-9 molecules filled the gaps, resulting in closure of the gaps. (*D*) The arrows in *A* and *B* indicate the positions on the preformed peptide nanofilaments mechanically manipulated by the tip of atomic force microscope. Section analysis of the double-layered nanofilaments that were repaired. The experiment was carried out on mica under an aqueous solution containing 50 mM $MgCl_2$.

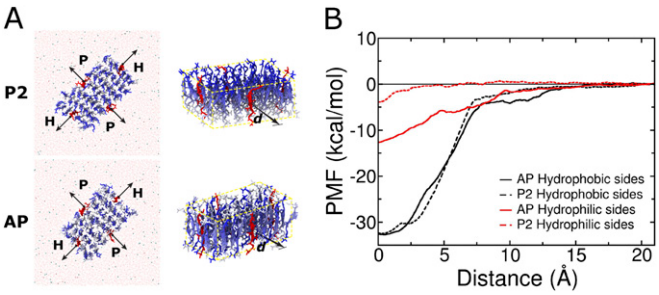

Fig. S2. Potential of mean force (PMF) of peptide binding reactions in two proposed assembly configurations [antiparallel (AP) model vs. parallel 2 (P2) model] in the top layer. (*A*) Simulation setups with 7 × 7 GAV-9 peptide islands, used previously for monolayer growth, in respective P2 (up) and AP (down) model configurations in 100.0 mM $MgCl_2$ bulk solution of explicit waters. In our steered molecular dynamics (SMD), an attempt was made to pull off a central peptide in each side (edge) from the equilibrated position along the surface normal, with a constant velocity of 0.5 Å/ns by means of an external spring with a force constant (k) of 5.0 kcal/mol, with the remaining island weakly restrained with harmonic potentials on C_α atoms (k = 5.0 kcal/mol). The four edges of the preassembled island are in different environments, depending on their hydrophobic or hydrophilic exposure. The two edges on the longer axis [indicated as hydrophobic (H) edges] expose hydrophobic side chains, whereas the other two edges on the shorter axis [indicated as hydrophilic (P) edges] expose hydrophilic backbones. We performed SMD for the central peptide of each edge five times, with an aggregate of >1.7 μs of molecular dynamics simulations. The PMF for each edge type (H and P) was then calculated with the Jarzynski equation (1, 2) by averaging over all trajectories obtained from both edges in the same edge type. (*B*) Binding free energy profiles in two different peptide arrangements (P2 and AP models). We found that peptide bindings on H sides are significantly more stable than bindings on P sides, which is concordant with our previous findings that the hydrophobic interaction dominates the longitudinal growth of GAV-9 nanofilaments on mica (3). The binding free energies are also comparable on the H edges for both the AP and P2 models ($\Delta G_{bind} \approx -32$ kcal/mol). On the contrary, interactions along the P edges (i.e., transversal lateral directions) are more sensitive to the peptide arrangement. The AP model stabilizes the binding by ∼12 kcal/mol for a single peptide, whereas the P2 model stabilizes the binding by only ∼4 kcal/mol. This indicates that the ionic strength (i.e., ∼6 Å of Debye length) might not be enough to screen out electrostatic repulsion in the P2 model between short-distanced (<5 Å) peptides along the transversal P sides (linked by backbone hydrogen bonds), although for the relatively long-distanced (∼10 Å) peptides along the longitudinal direction (due to bulky side chains), the electrostatic repulsion is no longer a major force due to the longer distance and more effective screening; thus, both the AP and P2 models give similar binding affinities due to their comparable hydrophobic interactions. Our PMF results therefore further support that the AP model is thermodynamically more stable than the P2 model for the upper layers, which largely comes from the aid of a more supportive transversal lateral interaction in its antiparallel arrangement.

1. Jarzynski C (1997) Nonequilibrium equality for free energy differences. *Phys Rev Lett* 78(14):2690–2693.
2. Park S, Khalili-Araghi F, Tajkhorshid E, Schulten K (2003) Free energy calculation from steered molecular dynamics simulations using Jarzynski's equality. *J Chem Phys* 119(6):3559–3566.
3. Kang SG, et al. (2013) Hydrophobic interaction drives surface-assisted epitaxial assembly of amyloid-like peptides. *J Am Chem Soc* 135(8):3150–3157.

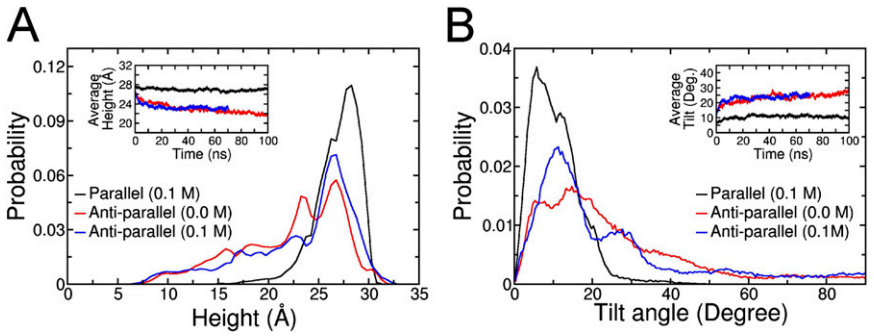

Fig. S3. Average heights (*A*) and tilting angles (*B*) of the peptide assemblies at the sublayer. We configured two possible morphologies depending on the relative orientation of GAV-9: (*i*) parallel mode: GAV-9 peptide are arranged to have the same N-terminal–to–C-terminal (N-to-C) orientation on mica, and (*ii*) antiparallel mode: GAV-9 peptides are arranged to have antiparallel orientations between themselves. In two testing salt concentrations of 0.0 and 0.1 M $MgCl_2$, the average height and tilt angle of the antiparallel mode ended up at 2.3–2.4 nm and 25°, respectively, with much wider distributions, whereas the parallel mode has much narrow distributions with a ∼2.8-nm height and a ∼10° tilt angle from the surface normal. Our results propose that the parallel mode is more plausible in the first layer regardless of the salt concentration. Overall, in the first layer, a direct interaction with the mica surface plays an important role in determining assembly structures, whereas from the second layer, the intralayer peptide–peptide interaction becomes dominant to drive the assembly. Deg., degree.

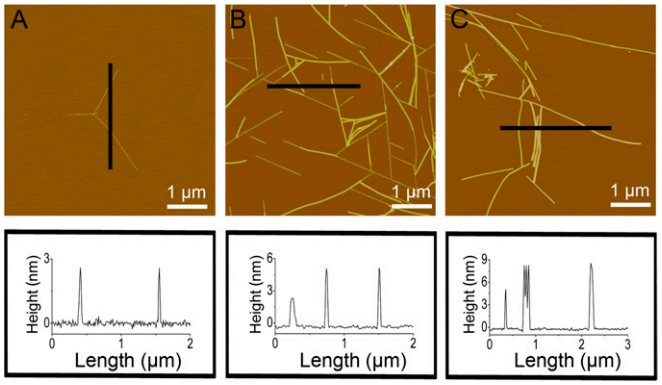

Fig. S4. AFM height images and section analysis of the GAV-9 assemblies under aqueous solutions containing additional concentrations of $MgCl_2$: 0 mM (*A*), 20 mM (*B*), and 200 mM (*C*), respectively.

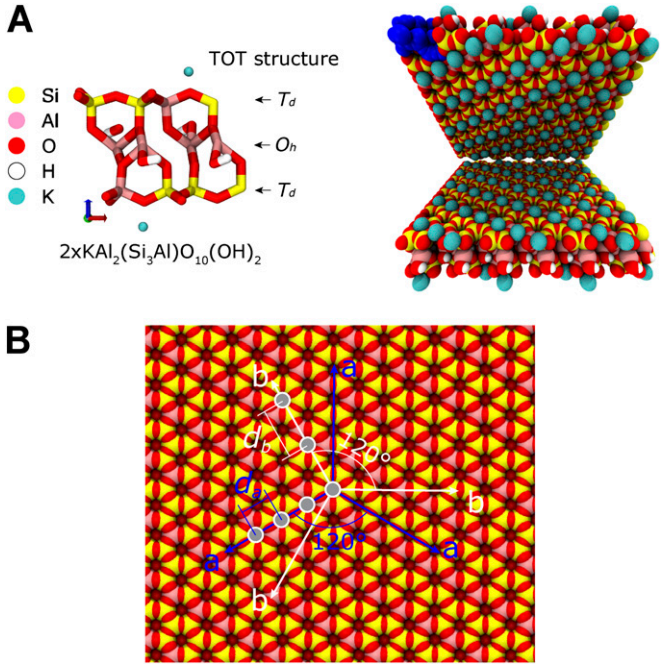

Fig. S5. Surface structure of muscovite mica. (*A*) Muscovite (001) surface was built by periodically extending two unit cells of the monoclinic C2/c 2M1 crystal structure [i.e., 2× $KAl_2(Si_3Al)O_{10}(OH)_2$] as a base (1). (*Left*) Subfigure illustrates the base structure, showing the T_d-O_h-T_d (TOT) triad structure along the surface normal. The surface construction is guided by the Loewenstein Al-avoidance rule (2, 3) to avoid distortions in Al-octahedra in the O_h layer, where more than one oxygen atom bonded to Al in the O_h layer is not allowed (to link Al in the T_d layers). The negatively charged T_d layers, composed of a 1:3 ratio of Al/Si, are neutralized with surface K^+ ions located on top of Si_4Al_2. (*Right*) Subfigure illustrates one example structure by extending the base structure by $6 \times 10 \times 2$ times along the *x*, *y*, and *z* directions, respectively. The interface between two slabs is stabilized by tightly packing the empty Si_5Al_1 sites and K^+ ions from both surfaces. (*B*) Detailed surface structure shows 2D crystallographic directions and possible peptide binding sites. The crystallographic a- and b-directions are indicated with blue and white arrows, respectively, with each spaced at 120°. The a- and b-directions are characterized by their different unit cell separations: $d_a = 0.52$ nm and $d_b = 0.92$ nm. In low-salt concentrations, epitaxial growth patterns of 120° each between self-assembled nanofilaments, which were presumably the most stable arrangements, were indeed most commonly observed on mica (4) (Fig. S4*A*). Our structural analysis showed that the crystallographic anisotropy (a- and b-directions) of mica surface can synergistically stabilize peptide self-assembly by facilitating short-distanced (~0.5 nm) backbone hydrogen bonds along the a-direction and relatively long-distanced (~0.9 nm) side chain hydrophobic interactions along the orthogonal b-direction. Our simulations then revealed a highly ordered β-stranded secondary structure as exposing hydrophilic backbone atoms to the a-direction and hydrophobic side-chains to the b-direction. In the following study, we also demonstrated that the longitudinal assembly grows along the b-direction, driven by energetically more favorable hydrophobic interaction, whereas the a-direction controls the transversal lateral growth via interpeptide backbone hydrogen bonds (5). This indicates that the linear assembly patterns shown in the AFM experiment grow epitaxially along the crystallographic b-direction on mica surface, often with 120° deviations from each other, particularly under low-salt concentrations.

1. Kuwahara Y (1999) Muscovite surface structure imaged by fluid contact mode AFM. *Phys Chem Miner* 26(3):198–205.
2. Loewenstein W (1954) The distribution of aluminum in the tetrahedra of silicates and aluminates. *Am Mineral* 39(1-2):92–96.
3. Brigatti MF, Guggenheim S (2002) Mica crystal chemistry and the influence of pressure, temperature, and solid solution on atomistic models. *Micas: Crystal Chemistry and Metamorphic Petrology* 46:1–97.
4. Kang SG, et al. (2012) Molecular mechanism of surface-assisted epitaxial self-assembly of amyloid-like peptides. *ACS Nano* 6(10):9276–9282.
5. Kang SG, et al. (2013) Hydrophobic interaction drives surface-assisted epitaxial assembly of amyloid-like peptides. *J Am Chem Soc* 135(8):3150–3157.